Available online at www.sciencedirect.com
SCIENCE DIRECT®
Journal of Magnetic Resonance 172 (2005) 222–230
JMR Journal of Magnetic Resonance
www.elsevier.com/locate/jmr

An object-oriented designed finite-difference time-domain simulator for electromagnetic analysis and design in MRI—applications to high field analyses

Q. Wei[a], F. Liu[a], L. Xia[b], S. Crozier[a,*]

[a] The School of Information Technology and Electrical Engineering, The University of Queensland, St. Lucia, Brisbane, Qld., 4072, Australia
[b] Department of Biomedical Engineering, Zhejiang University, Hangzhou, China

Received 6 September 2004; revised 22 October 2004
Available online 21 November 2005

Abstract

This paper presents a finite-difference time-domain (FDTD) simulator for electromagnetic analysis and design applications in MRI. It is intended to be a complete FDTD model of an MRI system including all RF and low-frequency field generating units and electrical models of the patient. The program has been constructed in an object-oriented framework. The design procedure is detailed and the numerical solver has been verified against analytical solutions for simple cases and also applied to various field calculation problems. In particular, the simulator is demonstrated for inverse RF coil design, optimized source profile generation, and parallel imaging in high-frequency situations. The examples show new developments enabled by the simulator and demonstrate that the proposed FDTD framework can be used to analyze large-scale computational electromagnetic problems in modern MRI engineering.

Keywords: Electromagnetic field; FDTD; Biological tissue model; Object-oriented design; RF coil; B_1 field; High field MRI

1. Introduction

The numerical modeling of electromagnetic fields (EMFs) generated by MRI coils presents a difficult computational problem, particularly those fields within a patient. Several methods, including analytic [1–3], finite element [1], and finite-difference [4] algorithms have been developed for the evaluation of EMFs excited by gradients or radiofrequency (RF) coils. Among them, the finite-difference time-domain (FDTD) method [1,5–11] has been used extensively for MRI applications. This is because FDTD method has a distinct advantage in handling field-sample interactions and these interactions are becoming more important as MRI moves to high field strengths.

We have developed a series of FDTD schemes [7–11], which can be used to analyze low-frequency problems (gradient fields) as well as high-frequency RF problems. We are attempting to generate a complete FDTD model of an MRI system including all field generating units and an electrical model of a patient. This might lead to a better understanding of the fields within patients and general temporal field behavior during an MRI scan, thus offering insight into coil design. To this end, we have designed a fully three-dimensional FDTD simulator which integrates our previously developed algorithms and includes several improvements such as automated handling of perfectly matched layer (PML) boundary conditions and some source models [11].

By enabling all FDTD simulations, from gradient to RF fields, in a single platform interactions with the patient and other accessories can be analyzed and

* Corresponding author. Fax: +61 7 3365 4999.
E-mail address: Stuart@itee.uq.edu.au (S. Crozier).

1090-7807/$ - see front matter © 2004 Elsevier Inc. All rights reserved.
doi:10.1016/j.jmr.2004.10.009

accounted for. For example, the eddy currents generated in an RF resonator due to gradient switching can be evaluated while patients SARs are calculated. This interplay of components and fields provides useful insight into system design.

Computationally intensive numerical software/tools have become necessary to handle the increasing complexity of EMF problems in MRI, particularly at high field strengths. For a practically useful implementation, efficient software engineering of the appropriate algorithms is very important. The analysis and design of EMF computation has generally been carried out using procedural approaches, which limit the reuse of certain parts of the procedure in another project. Compared with traditional methodologies, contemporary software engineering concepts like object-oriented design (OOD) have some advantages in handling complicated data modeling and numerical algorithms [12–14], and help to create modular, user-friendly, and extensible software. We therefore architect this simulator with the assistance of OOD techniques and philosophies. In this work, the design procedure is described and demonstrates how OOD can lead to well-organized field calculation tool. The numerical scheme has been employed to a variety of gradient and RF field analyses. In particular, several strategies have been attempted within the simulation package to understand and attempt to overcome the B_1-field inhomogeneity problems in tissue at high frequencies.

2. Methodology

2.1. FDTD method

2.1.1. Standard FDTD for RF field calculations

The FDTD methodology [15] is derived from Maxwell's curl equations $\mu\partial\vec{H}/\partial t = -\nabla\times\vec{E}$, $\varepsilon\partial\vec{E}/\partial t = \nabla\times\vec{H} - \sigma\vec{E} - \vec{J}_{\text{source}}$, where $\vec{E}$ and $\vec{H}$ are the electric and magnetic field intensities and μ, ε, and σ are the space-dependent permeability, permittivity, and conductivity of the medium, respectively. $\vec{J}_{\text{source}}$ is the impressed current density. Employing a Yee-algorithm for the discretization of (1) in Cartesian coordinates results in a set of algebraic time-stepping relations which may be written in a compact form as

$$\begin{cases} \vec{H}^{n+1/2} & = c_{h1}\vec{H}^{n-1/2} + c_{h2}[D][\Pi]^T \\ \vec{E}^{n+1} & = c_{e1}\vec{E}^{n+1/2} + c_{e2}[D][\Xi]^T + c_{e3}\vec{J}^{n+1/2} \end{cases} \tag{1}$$

with the definition

$$[D] \triangleq [D_x, D_y, D_z], \quad [\Xi] \triangleq [\hat{x}\times\vec{E}^n\hat{y}\times\vec{E}^n\hat{z}\times\vec{E}^n],$$
$$[\Pi] \triangleq [\hat{x}\times\vec{H}^{n+1/2}\hat{y}\times\vec{H}^{n+1/2}\hat{z}\times\vec{H}^{n+1/2}], \tag{2}$$

where the superscript denotes the time step $t = n\Delta t$, and D_x, D_y, D_z are difference operators. The coefficient terms are space-dependent diagonal tensors whose components are defined by

$$c_{h1} = 1, \quad c_{h2} = -\Delta t/\bar{\mu}, \quad c_{e1} = \frac{2\bar{\varepsilon}_i - \bar{\sigma}_i\Delta t}{2\bar{\varepsilon}_i + \bar{\sigma}_i\Delta t},$$
$$c_{e2} = \frac{2\Delta t}{2\bar{\varepsilon}_i + \bar{\sigma}_i\Delta t}, \quad c_{e3} = -\frac{\Delta t}{\bar{\varepsilon}_i}, \tag{3}$$

for $i = x$, y or z. The overbar $(\bar{\cdot})$ characterizes the local averaged values of the constitutive parameters over Yee-cells.

The EMFs in the spatial domain can be tracked through (1). The excitation is introduced by specifying the current density or input voltage at grid points that coincide with the source positions. Artificial truncations are placed at the outer boundary of the problem domain which is placed a suitable distance from the investigated zone. One of these advanced boundary conditions is Berenger's PML[15]. The steady-state EMF solution can be achieved by a peak detection approach or an DFT method [1].

2.1.2. Low-frequency algorithm for gradient field calculation

FDTD is inherently a high-frequency algorithm for EMF calculations. The above formulations can be employed directly into an RF field analysis; however, there are some technical issues when the standard FDTD scheme is applied to the low-frequency problems such as gradient switching. Direct calculation turns out to be impractical and modified FDTD implementations have to be devised. To circumvent the unacceptable computation time required to use conventional FDTD technique at low frequencies, an effective Fourier analysis-based time/frequency numerical conversion technique [7,9] has been proposed. As source injection in the FDTD simulation plays a crucial rule in obtaining accurate solutions, a voltage source model [8] was constructed by making use of the derivative of the input source waveform. Recently, a distributed equivalent magnetic current (DEMC)-based FDTD method [11] has been investigated to further enable complex, low-frequency source modeling.

2.2. Biological tissue model

The electromagnetic data of the human body and Sprague–Dawley rat used in this work was obtained from the US Air Force Research Laboratory (http://www.brooks.af.mil/AFRL/HED/hedr/). There are a total of 40 segmented tissues in the human model and 12 tissue types in the rat phantom. The original spatial resolution of the human and rat model is approximately 1 mm. For FDTD computations, the models can be mapped onto a defined grid with volume-averaged dielectric properties.

2.3. Object-oriented design

In OOD, inheritance and polymorphism are two key features. inheritance is a mechanism that permits the expression of common characteristics among classes; it simplifies the definition of classes that are similar to others as the descendant inherits automatically all the data and methods of its ancestor. Inheritance is one of the most important features that enables the reusability of code in OOD. polymorphism is the ability to use the name of a function to represent different implementations of it. In our FDTD simulator, the class hierarchy design relies heavily on inheritance and polymorphism by means of virtual methods [16].

2.3.1. Class description

In this OOD system, computational electromagnetics problems are handled through class construction. Class structure is designed to provide coherent mapping between the theoretical aspects of field analysis and the software implementation. Here, we describe how to identify or define those classes in our problem space.

As mentioned before, in FDTD analysis, the whole domain is truncated and subdivided into many adjacent cells, which converts the calculation of fields from the whole domain to a cell domain. In this fashion, the cell analysis becomes the key point, and *CELL* class is the base of all classes of objects that is used by the assembler/solver. In each cell, three E-field components, three H-field components, and constitutive electromagnetic parameters are the basic member variables; the six EMF-update operations (see (1)) are the essential methods. The basic definition of *CELL* class is

```
class CELL{

protected:
float _ex, _ey, _ez;   // E-field values
float _hx, _hy, _hz;   // H-field values
float epr, sig;    // relative permittivity & conductivity
// FDTD updating coefficients
float _cEx1, _cEx2, _cEy1, _cEy2, _cEz1, _cEz2, _cH1, _cH2;
int _Eneighbours[3], _Hneighbours[3]; // indicates
    neighbor type

public:
Cell();    // constructor
void setEneighbour();    // set neighbor's status
void setHneighbour();
float getEvalue();    // get E-field values
float getHvalue();    // get H-field values

virtual char* getType() {return cellType;} // to get cell
   type for different objects
// set coefficients of FDTD update equations
virtual void setEcoefficients( float *CE );
virtual void setHcoefficients( float *CH );
// Update Maxwell's curl equations
virtual void updateEx( float dhy, float dhz );
virtual void updateEy( float dhx, float dhz );
virtual void updateEz( float dhx, float dhy );
virtual void updateHx( float dey, float dez );
virtual void updateHy( float dex, float dez );
virtual void updateHz( float dex, float dey );

~Cell();    //destructor

};
```

In this definition, all the member variables and functions are used to realize the FDTD solver, some of which will be explained further in the next section.

In MRI engineering, a typical computational domain can be represented by Fig. 1. The EMF objects include free space (air), source (coil current or voltage source), and biological objects (load), RF circuits and boundary condition including the perfect conductor (PEC), surface impedance boundary condition (SIBC) [15], and artificial boundaries (PML), etc. Hence, the main domain can be split into several sub-domains. Several derived sub-classes from the *CELL* class are identified, i.e., *CAIR* is defined for the free space; *CSOURCE* relates to the input source; *CLOAD* handles the imaged sample/load; *CCIRCUIT* considers the RF circuits and dielectrics; *CPML* and *CPEC* are basic boundary conditions. *CELL* class is the abstract which contains the values and operation functions shared by all these sub-classes, a group of virtual functions are defined therein, which provide the flexible and extensible way for assisting the sub-classes to perform their functions. Fig. 2 describes the class hierarchy and some basic overloaded methods in these subclasses.

This class hierarchy has good inheritance performance. Each sub-class is highly decoupled, however, in that changing any sub-class does not affect the others.

Overloading or overriding virtual functions realizes the implementation of polymorphism. As shown in

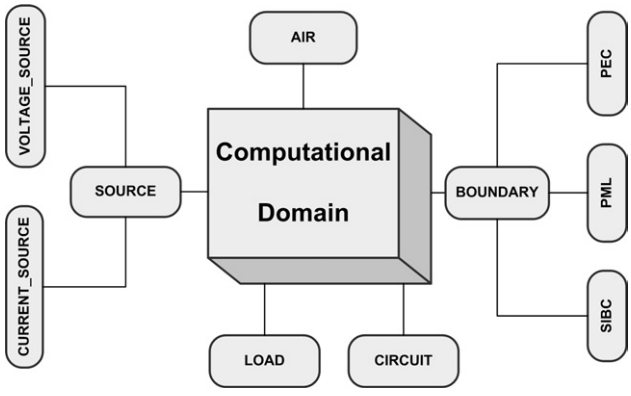

Fig. 1. The configuration of the FDTD computational domain in MRI. (PEC, perfect conductor; PML, perfect matched layer [15]; SIBC, surface impedance boundary condition [15].)

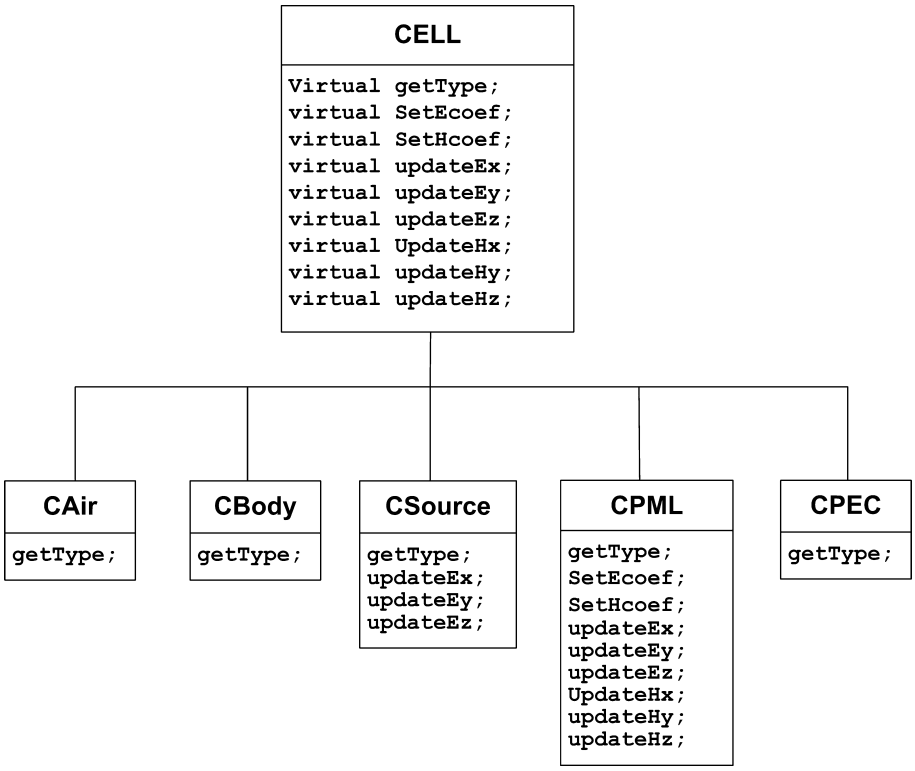

Fig. 2. The class hierarchy in the FDTD simulator.

Fig. 2, virtual functions are heavily used in our sub-class design. To provide a more substantial example to demonstrate this process, a member function updateEx() is illustrated here. This method is implemented differently in these sub-classes

For *AIR*, the following format can be used

```
inline void CAIR::updateEx( float dhy, float dhz ) {
  _ex = _cEx1*_ex+_cEx2*( dhz − dhy );

}
```

For *SOURCE*, the corresponding operation is

```
inline void CSOURCE::updateEx( float dhy, float dhz)
{
_source = SourceFunction( t );
_ex = _cEx1*_ex + _cEx2*( dhz − dhy ) + _source;
}
```

For *PML*, the split-version has been employed as

```
inline void CPML::updateEx ( float dhy, float dhz ) {
_Exy = _cExy1*_Exy + _cExy2*dhz;
_Exz = _cExz1*_Exz + _cExz2*dhy;
_ex = _Exy + _Exz;

}
```

For *PEC*, the field values are all zero and hence need not be updated.

Similarly, many other member methods are overloaded. The overhead imposed by these virtual functions is small compared to the time spent evaluating the functions themselves and so it is a good compromise between flexibility and efficiency.

Finally, to manage all the above mentioned sub-classes, another class called *DOMAIN* has also been defined in this simulator.

2.3.2. Implementation

The FDTD simulator is coded using C++ language with the capability of upgrade and expansion. Using this object-oriented programming language allows efficient project management and code reuse in cross-platform development.

The FDTD execution procedure is shown in Fig. 3. Initially all field values are set to zero or a known initial value. Next, a looping procedure starts to discretely solve the EMFs as time increments. The output data is organized and analyzed in a post-processing module.

In the implementation, before using the FDTD solver, all the system parameters such as the human model and source data are obtained from files and/or through a dedicated user interface (see Section 2.4). For each cell, the associated properties and its neighbor information such as cell type and electrical parameters are obtained and indexed by pointers. Here, each base class pointer can point to its derived class. During implementation, each pointer refers to an appropriate sub-class instance based on corresponding conditions. To accelerate the updating procedure of all electromagnetic components,

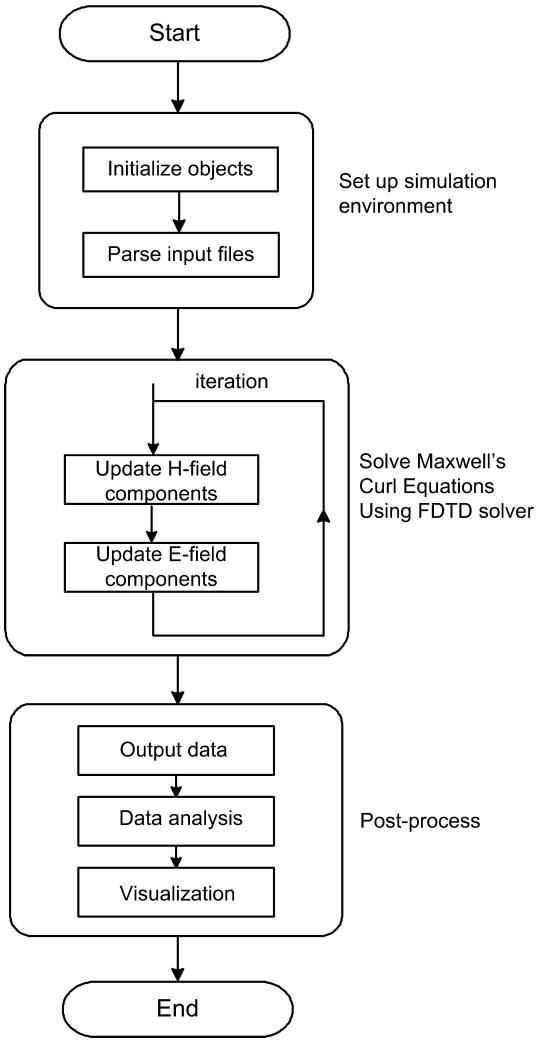

Fig. 3. Flow chart of the FDTD simulation procedure.

frequently used coefficients are pre-computed and stored as local private variables in each cell. This can be achieved by introducing one or more methods to invoke those pre-computing processes. Before FDTD iteration, setting the neighbor status is required as the determination of objects of the surrounding cells is also a critical factor influencing the computational time. After a series of pre-processing steps, it is possible to update field values inside each cell rather than looking for the most commonly required information as it appears in standard procedure-oriented programming. That is, large "if-then-else" chains are avoided by using the polymorphism property. This is one critical benefit of OOD for FDTD calculations.

As previously mentioned, in this work we have also redesigned the PML structures. Implementing a PML usually offers high performance but requires a considerable amount of memory. Within the OOD framework, the implementation of PMLs is simplified due to the class generation and because the need to generate "split" EMF components [7–11] is significantly reduced. The computational cost is therefore also significantly reduced for 3D problems. For example, this method saves about 40% of computation time and memory for the simulations of Section 3.

2.4. Interfacing, data process, and visualization

For interactive design and monitoring of the corresponding simulation procedure, a graphical user interface (see Fig. 4) has been developed. It provides a clear wizard to assist users to handle their own system data/parameters for the FDTD solver. To post-process the computed data, some external numerical libraries and C++ toolkit can also be incorporated into the framework. The visualization of the output data is handled using openGL or by calling other software such as Matlab.

3. Simulations

Before embarking on the study of biological body–field interactions, it is essential to verify the code against analytic solutions. We have studied an "equivalent" head load, which was a seven-layered, concentric spherical volume conductor (for phantom details, see [3]). In this case, a typical current loop was considered as source and the induced fields inside the model were calculated using Debye-potential-based method [3], quasi-static finite-difference method [4], and low-frequency FDTD algorithms [7,11] employed in this simulator, respectively. The results corresponded well to those previously published [3], demonstrating that the simulator is useful for the analysis of gradient field problems such as eddy currents in patients or magnets.

We next evaluate the use of the simulator for high-field problems. High magnetic field/(frequency) technology has brought considerable engineering challenges in the form of ancillary hardware, particularly the RF resonator [17]. We have analyzed the tissue–RF field interactions using a ReCav coil [18] at 11 T. The FDTD results confirmed the experimental observations that tissue/field interactions distort brain images. With the help of this simulator, we now illustrate some techniques that could be potential solutions to high-frequency RF problems.

First, we evaluated an unconventional concept for a volume coil. Fig. 5 shows an example design of a coil structure obtained using an inverse method [19] at 4 T (170 MHz). The coil-generated B_1 field patterns for the empty case are shown in Fig. 5A. In this case, further investigations were carried out and the coil current profile was reconfigured with and without de-emphasized B_1 target fields [21]. Figs. 5B and C show the calculated signal intensity (SI) [20] when the coil was loaded with a cylindrical phantom ($\varepsilon_r = 78$, $\sigma = 0.4$). From the simulation results, it can be seen

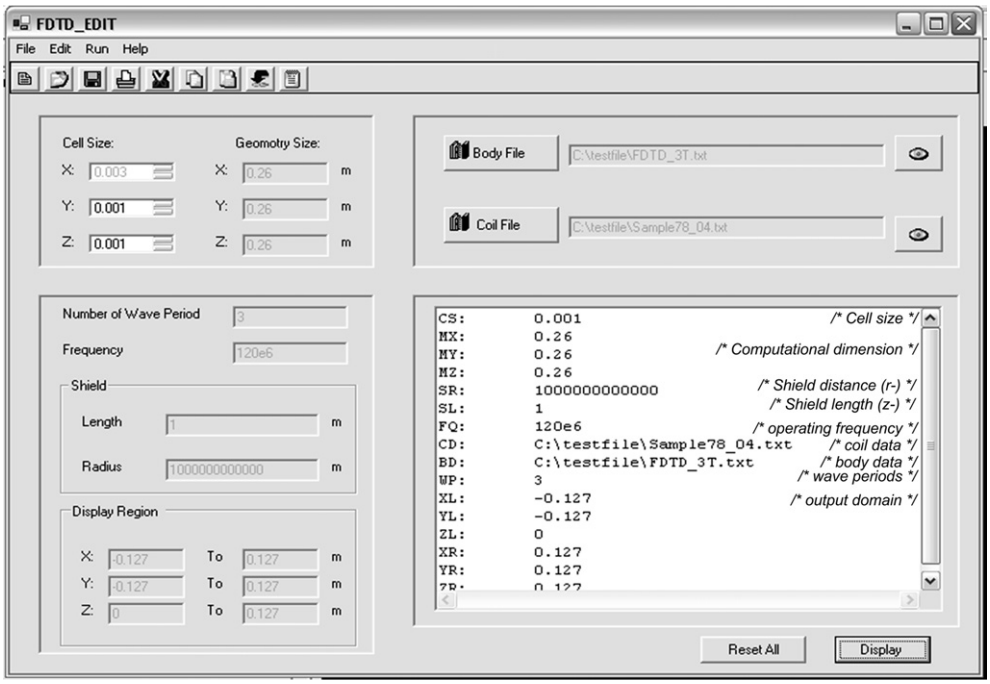

Fig. 4. User interface of the FDTD simulator.

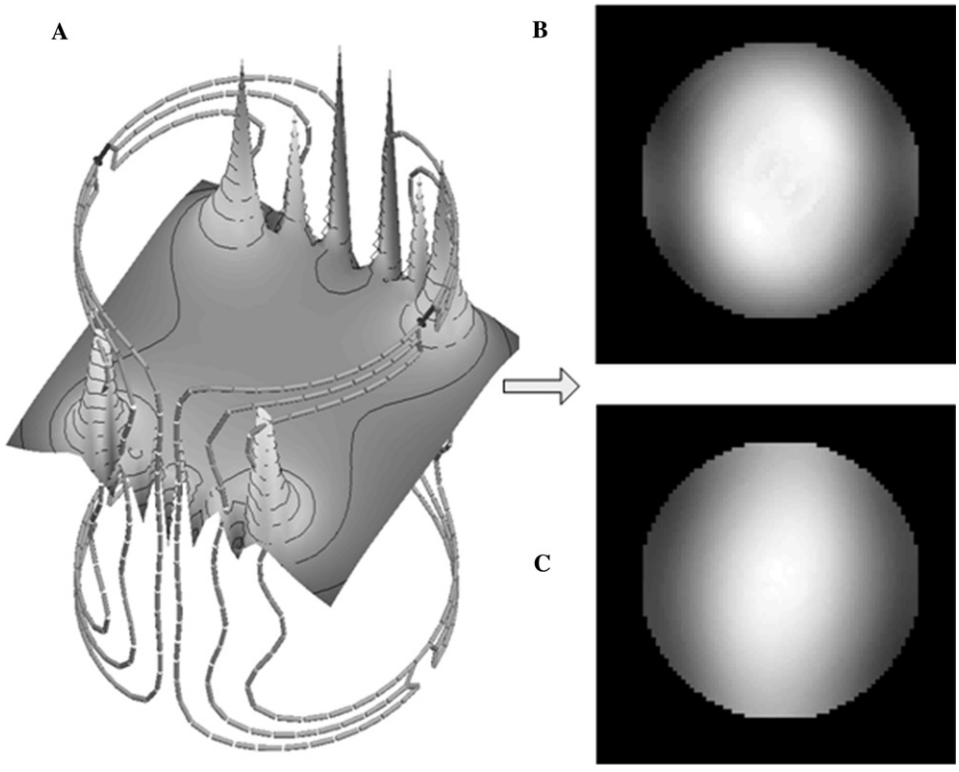

Fig. 5. The simulation of the inverse-method designed RF coil at 4 T using de-emphasized target fields. (A) The coil structure and the $|B_1|$ field map at empty case; (B) Simulated signal intensity map at $z = 0$ plane loaded with cylindrical phantom ($\varepsilon_r = 78$, $\sigma = 0.4$) without de-emphasis; (C) Simulated signal intensity map at $z = 0$ plane loaded with cylindrical phantom ($\varepsilon_r = 78$, $\sigma = 0.4$) with de-emphasis.

that the de-emphasis method does help in decreasing the aberrant central bright region caused by field/tissue interactions at this frequency.

We then investigated the strategy of improving the transmit B_1-field homogeneity through active control of source profiles [24], i.e., to tailor the RF amplitudes

and phases applied individually to the rungs of a resonator with the use of an optimization method. In this study, an elegant optimization algorithm (subspace trust-region interior-reflective (STIR) method [22]) was employed to determine the rung currents on a 12-element, shielded birdcage coil (see Fig. 6) operating at 170, 300, and 470 MHz. In the optimization procedure, the first step was to employ FDTD to calculate the sensitivity profile of each rung loaded with a 2D axial-sliced head model; the second step was to implement STIR algorithm to search for improved uniformity of RF field inside the sample. During the iterative optimization, superposition of the sensitivity profiles produced by complex current amplitudes for each rung was employed to evaluate the B_1 field and hence intensive FDTD calculations were avoided. The manner in which a target function is defined is critical for practical optimization as the phase components of B_1 field need to be taken into account in high-frequencies analyses [2]. Fig. 6A shows the model setup and Fig. 6B shows the comparison results for B_1 field distribution before and after optimization. From these results, it can be seen that this transceive optimization is capable of improving the uniformity of the RF field. For these cases, about 85% of the B_1-inhomogeneity caused by loading effect can be compensated for by the optimized rung currents. In this preliminary work we restrict ourselves to 2D scenarios [23], but the formalisms should be easily adapted to other situations such as 3D volume resonator and phased-array systems. Optimal RF pulse modulation schemes are also being investigated for use with these structures. The use of a convenient simulator, such as that described herein, is critical to the success of this work.

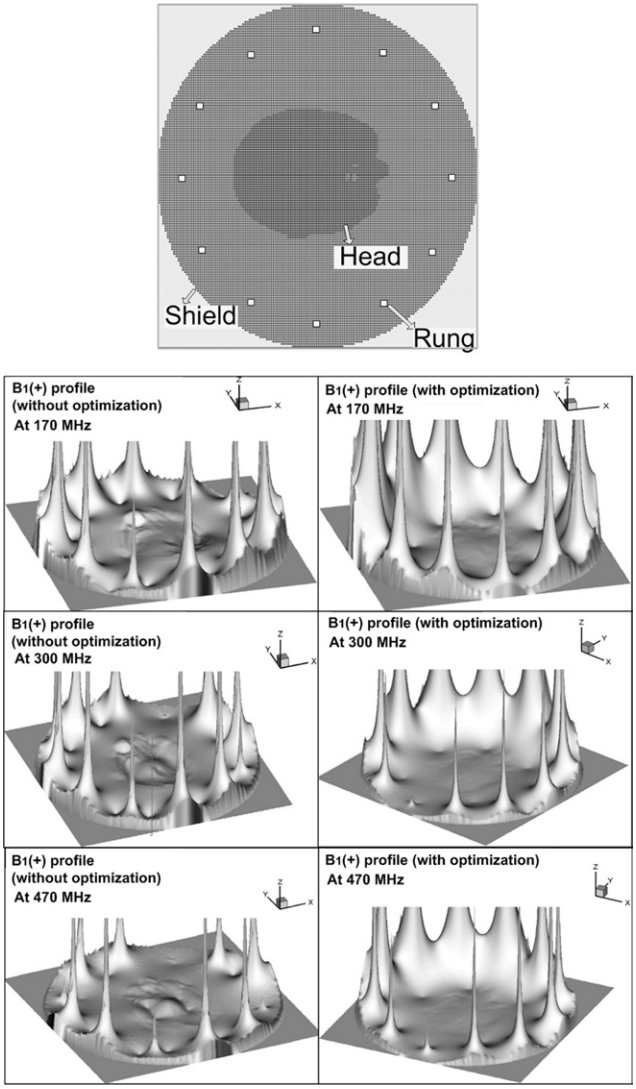

Fig. 6. Optimization of the source profile for a shielded birdcage resonator. (A) The simulation setup (number of elements: 12; coil radius: 37 cm; shield radius: 45 cm; head model size: 18 cm × 24 cm; FDTD cell-size: 3 mm); (B) Comparisons of the B_1 field map before and after optimization.

It is believed that phased-array coils operated as transceiver could be a possible solution for high-frequency RF systems [24]. Here phased-array coils for chest imaging (see Fig. 7) [25] are studied. In this simulation, we generate a transceive, focused system with SENSE reconstruction using 8-element transceiver torso phased-array coil as shown in Fig. 7A. The RF field/torso interaction was analyzed with the FDTD simulator. After the FDTD simulations, the sensitivity profile of each coil (Fig. 7B) was obtained to reconstruct the SENSE image [26] (see Figs. 7C and D). This simulation shows that the parallel imaging could be employed for high field MRI but requires further investigation.

Finally, for high-field systems, the RF safety issue was considered with the simulator. We have developed a thermal model to evaluate temperature rise in the Sprague–Dawley rat due to electromagnetic energy deposition at high-field strengths ranging from about 11.75–23.5 T (0.5–1 GHz) within a 8-element birdcage resonator. The Pennes bioheat transfer equation was approximated by finite difference method [18]. The simulations (see Fig. 8) showed that the temperature rise can become quite significant in local body regions under some circumstances. This model is also useful for the analysis and optimization of hyperthermic tumor treatment.

4. Discussion

From the above case studies, it can be seen that this simulator allows us to analyze many sorts of MRI coil structures, test new designs under a common software environment and thereby create a rapid, theoretical prototyping facility. In particular, new developments in high-frequency RF engineering have been prototyped using the simulator. There is certainly a trade-off

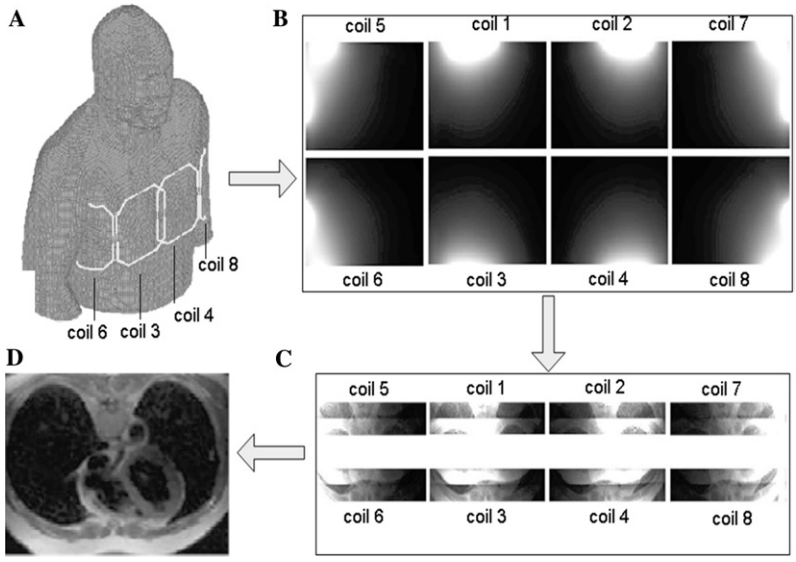

Fig. 7. The simulation of the transceive torso phased-array coil at 2 T. (A) The coil structure and the human model; (B) simulated sensitivity profiles with focused B_1 field near the heart region; (C) the simulated, aliased chest images using the parallel imaging scheme; and (D) the SENSE reconstructed chest image.

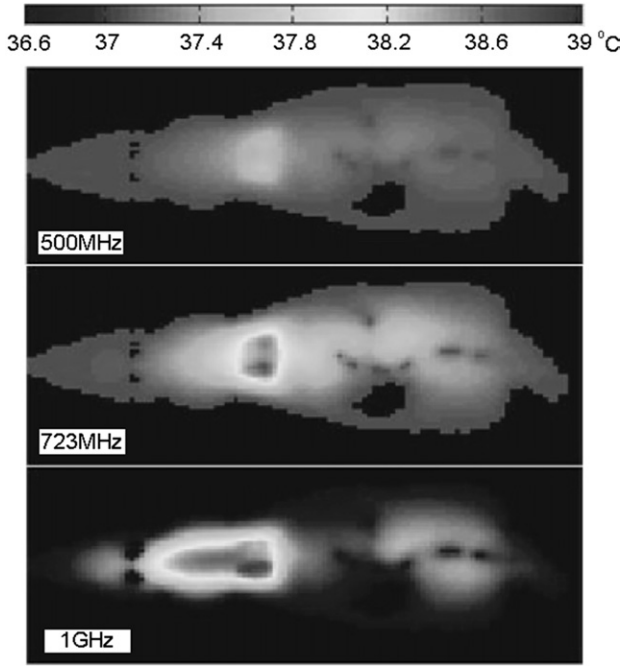

Fig. 8. Temperature map simulations inside a rat phantom (x–z cross section) at high frequencies using an RF pulse duration of 3 ms and a total of eight pulses in a fast spin echo type sequence, the value of TE is estimated as 24 ms, while TR $\approx$ 400 ms.

between computational efficiency, programming efficiency and software flexibility. As described above, however, many strategies can be devised to improve the efficiency of an FDTD solver for specific cases [14]. In particular, the class definition in this simulator assists in the potential parallel implementation of the yee-algorithm. We are currently investigating the parallel implementation of the simulator with the help of MPI techniques in supercomputer systems. While there is no significant computational penalty associated with the use of OOD in the development of field calculation software, the major benefit is that a logically expandable platform is developed.

The FDTD solver can also be combined with other field calculation programs such as FEKO (http://www.feko.co.za). One option is for the coils to be modeled using method of moments (MoMs), and the biological load is handled within the FDTD simulator. The communication between these two solvers can be realized through an equivalent surface with careful design [15,27]. Recently, this simulator has been adapted into other biomedical imaging problems (such as implant identification) using total/scattered field formulations [15].

5. Conclusion

The precise evaluation of EMF distributions inside biological samples is becoming an increasingly critical design requirement in high field MRI engineering. In this work, a dedicated numerical tool architected using object-oriented computational modeling method is presented. The simulator provides a software platform in terms of a C++ class hierarchy which reflects the MRI physics and practical engineering problems. By enabling an FDTD simulator for this work, we are in a position to approach a complete model of an MRI system, including tissue-field interactions and the effect of EMFs on surrounding coils/conductors. This simulator has already been successfully applied to different RF coil anal-

yses particularly in high-frequency scenarios and we plan to expand the capabilities of the system. Appropriate avenues for the distribution of the software are being investigated.

Acknowledgment

Financial support for this project from the Australian Research Council is gratefully acknowledged.

References

[1] J.M. Jin, Electromagnetic Design and Analysis in Magnetic Resonance Imaging, CRC, Boca Raton, FL, 1999.
[2] D.I. Hoult, The sensitivity and power deposition of the high field imaging experiment, J. Magn. Reson. Imag. 12 (2000) 46–67.
[3] F. Liu, S. Crozier, Electromagnetic fields inside a lossy, multilayered spherical head phantom excited by MRI coils: models and methods, Phys. Med. Biol. 49 (2004) 1835–1851.
[4] F. Liu, H. Zhao, S. Crozier, On the induced E-field gradients in the human body for magnetic stimulation by gradient coils in MRI, IEEE Trans. Biomed. Eng. 50 (2003) 804–815.
[5] C.M. Collins, S. Li, M.B. Smith, SAR and B1 field distributions in a heterogeneous human head model within a birdcage coil, Magn. Reson. Med. 40 (1998) 847–856.
[6] T.S. Ibrahim, R. Lee, B.A. Baertlein, Y. Yu, P.M.L. Robitaille, Computational analysis of the high pass birdcage resonator: finite difference time domain simulations for high-field MRI, Magn. Reson. Imag. 18 (7) (2000) 835–843.
[7] F. Liu, S. Crozier, H. Zhao, Finite-difference time-domain based studies of MRI pulsed field gradient-induced eddy currents inside the human body, Concepts Magn. Reson. 15 (B) (2002) 26–36.
[8] H. Zhao, S. Crozier, F. Liu, A FDTD method for modeling the effect of switched gradients on the human body in MRI, Magn. Reson. Med. 48 (2002) 1037–1042.
[9] H. Zhao, S. Crozier, F. Liu, An analysis of the high-definition finite-difference time-domain methods, Appl. Math. Model 27 (2003) 409–419.
[10] F. Liu, S. Crozier, An FDTD Model for calculation of gradient-induced eddy currents in MRI system, IEEE Trans. Appl. Superconduct. 14 (2004) 1983–1989.
[11] F. Liu, S. Crozier, A distributed equivalent magnetic current based FDTD method for the calculation of E-fields induced by gradient coils, J. Magn. Reson. 169 (2004) 323–327.
[12] E.J. Silva, R.C. Mesquita, R.R. Saldanha, P.F.M. Palmeira, An object-oriented finite-element program for electromagnetic field computation, IEEE Trans. Magn. 30 (1994) 3618–3621.
[13] T.H. Jochimsen, M.V. Mengershausen, ODIN—object-oriented development interface for NMR, J. Magn. Reson. 170 (2004) 67–78.
[14] H.P. Langtangen, O. Munthe, Solving systems of partial differential equations using object-oriented programming techniques with coupled and fluid flow as example, ACM Trans. Math. Soft. 27 (2001) 1–16.
[15] A. Taflove, Computational Electrodynamics: The Finite-Difference Time-Domain Method, Artech House, Boston, 1995.
[16] B. Stroustrup, The C++ programming language, Addison Wesley, Boston, 2000.
[17] X. Hu, D.G. Norris, Advances in high-field magnetic resonance imaging, Annu. Rev. Biomed. Eng. 6 (2004) 157–184.
[18] F. Liu, B.L. Beck, B. Xu, S. Blackband, 11T MRI and numerical modeling of the excised, fixed human head, Concepts Magn. Reson. (in press).
[19] B.G. Lawrence, S. Crozier, D.D. Yau, D.M. Doddrell, A time-harmonic inverse methodology for the design of RF coils in MRI, IEEE Trans. Biomed. Eng. 49 (2002) 64–71.
[20] C.M. Collins, M.B. Smith, Signal-to-noise ration and absorbed power as functions of main magnetic field strength, and definition of 90 RF pulse for the head in the birdcage coil, Magn. Reson. Med. 45 (2001) 684–691.
[21] B. Xu, S. Crozier, Q. Wei, F. Liu, An inverse methodology for high frequency RF coil design with pre-emphasized B1 field in MRI, in: 26th Annual International Conference on IEEE Engineering, EMBS, San Francisco, 2004.
[22] M.N. Branch, T.F. Coleman, Y. Li, A subspace, interior, and conjugate gradient method for large-scale bound-constrained minimization problems, SIAM J. Sci. Comput. 21 (1999) 1–23.
[23] D.K. Spence, S.M. Wright, 2-D full wave solution for the analysis and design of birdcage coils, Concepts Magn. Reson. 18 (B) (2003) 15–23.
[24] R.G. Pinkerton, E.A. Barberi, R.S. Menon, Noise properties of a NMR transceiver coil array, J. Magn. Reson. 171 (2004) 150–155.
[25] B. Li, S. Crozier, F. Liu, Q. Wei, Transmitting focused B_1 field and SENSE reconstruction using 8-element transceiver torso phased array coil, in: 26th Annual International Conference on IEEE Engineering, EMBS, San Francisco, 2004.
[26] K.P. Pruessmann, M. Weiger, M.B. Scheidegger, P. Boesiger, SENSE: Sensitivity encoding for fast MRI, Magn. Reson. Med. 42 (1999) 952–962.
[27] Z. Huang, K. Demarest, R. Plumb, An FDTD/MoM hybrid technique for modeling complex antenna in the presence of heterogeneous grounds, IEEE Trans. Geosci. Remote Sens. 37 (6) (1999) 2692–2698.